Variations in Antigen−Antibody Association Kinetics as a Function of pH and Salt Concentration: A QSAR and Molecular Modeling Study†

Annick Dejaegere,‡ Laurence Choulier,§ Virginie Lafont,‡,§,|| Erwin De Genst,⊥ and Danièle Altschuh*,§

UMR 7175-LC1, CNRS/ULP, ESBS, Parc d'Innovation, Bld S. Brant, BP 10413, 67412 Illkirch Cedex, France, UMR 7104, Structural Biology and Genomics Department, Institut de Génétique et de Biologie Moléculaire et Cellulaire, CNRS/INSERM/ ULP, BP 10142 F-67404 Illkirch Cedex, France, and Laboratory of Cellular and Molecular Immunology, Department of Molecular and Cellular Interactions, Vlaams Interuniversitair Instituut voor Biotechnologie, Vrije Universiteit Brussel, Pleinlaan 2, 1050 Brussel, Belgium

Received May 26, 2005; Revised Manuscript Received August 18, 2005

ABSTRACT: The relationship between three environmental factors (ionic strength, pH, and temperature) and antigen−antibody binding kinetics was investigated using QSAR (quantitative structure−activity relationship) and molecular modeling approaches. The interaction used for this analysis is that between the camel antibody fragment cAbLys3 and lysozyme. Binding kinetics were measured using a Biacore 2000 instrument, at NaCl concentrations between 50 and 500 mM, at pH's between 5 and 10, and at temperatures between 15 and 30 °C, according to multivariate experimental designs. Variations in kinetic on- and off-rate parameters were up to 400- and 16-fold, respectively. Mathematical models that relate log k_{on} to experimental conditions were developed. They indicated an influence of all three factors, with a clear dependency between pH and NaCl concentration for their effect on k_{on}. These models were able to predict on-rate parameters under new experimental conditions. Titration calculations using continuum electrostatics were performed on the crystallographic structures of the isolated and bound proteins to gain structural insight for the on-rate enhancement observed at pH <6.5 and low salt concentrations. These calculations rule out electrostatic steering linked to global and/or local charge variations in the molecules as the factor responsible for the on-rate enhancement at low pH. His 111 of cAbLys3, located at the binding interface, can adopt two side chain orientations with different intramolecular contacts. The results of the calculations suggest an alternative mechanism whereby the conformation of the interfacial His 111 depends on the charge, and these differences in conformation may influence the solvation energy and the subsequent binding kinetics. Our results stress the complex relationship between environmental conditions and molecular binding properties.

Molecular interactions take place in a variety of environments but are typically investigated under only one or a few standard conditions (neutral pH, temperature between 20 and 37 °C, and physiological ionic strength), which may not be representative of the situations encountered in vivo or in vitro. A thorough description of a molecular interaction is not straightforward because many factors (temperature, pH, solvents, cofactors, etc.) may modify the binding properties. Furthermore, the factors sometimes act in a dependent manner; i.e., the effect on binding of one factor may depend on a second factor, thus complicating the experimental design and data interpretation. Another challenge is to explain the observed behaviors, which would help to predict the binding properties of new systems. Hypotheses for the effects of some factors can be proposed, and sometimes established by structural studies and/or computational approaches. For example, cofactors induce conformational changes in binding sites; temperature influences the entropy of the system, and pH influences the state of titrating sites in the protein, and therefore electrostatic interactions. Ionic strength also influences electrostatic interactions by shielding charges. In this work, we quantify the influence of three environmental factors (pH, NaCl concentration, and temperature) on antigen−antibody binding kinetics, as measured with a Biacore. We apply a multivariate QSAR[1] (quantitative structure−activity relationship) approach, which uses a statistical experimental design to extract the maximum amount of information from a minimum number of experimental runs. The approach allows the identification of factors that influence binding as well as dependencies between factors. We then investigate the possible structural causes

† This work was supported by the Centre National de la Recherche Scientifique, the Institut National de la Santé et de la Recherche Médicale, and the Université Louis Pasteur, Strasbourg, as well as by grants from the "Association pour la Recherche sur le Cancer" (ARC, Contracts 5173 and 3127) and from the French Ministry of Defense (Contract 20216 DSP/SREA/F). V.L. was supported by a fellowship from the Ministry of Defense.

* To whom correspondence should be addressed. Telephone: +33 (0)3 90 24 48 32. Fax: +33 (0)3 90 24 46 83. E-mail: altschuh@esbs.u-strasbg.fr.

‡ UMR 7104, CNRS/INSERM/ULP.

§ UMR 7175-LC1, CNRS/ULP.

|| Present address: Department of Biology, Johns Hopkins University, 3400 N. Charles St., Baltimore, MD 21218-2685.

⊥ Vrije Universiteit Brussel.

[1] Abbreviations: k_{on}, association rate parameter; k_{off}, dissociation rate parameter; QSAR, quantitative structure−activity relationship; RSM, response surface modeling; RU, resonance units.

10.1021/bi050986v CCC: $30.25
Published on Web 10/12/2005

for some of the experimental observations using molecular modeling approaches. The interaction system used for this study is that between the camel antibody fragment cAbLys3 and lysozyme (*1*, *2*).

The three factors that varied, pH, NaCl concentration, and temperature, are known to influence on- and/or off-rates. Solutions with extreme pH values are classically used to dissociate molecular complexes, and binding kinetics were shown to vary in the pH range of 4.5−8.5 (*3*), 4.1−7.4 (*4*), 5.5−9 (*5*), or 6.0−8.0 (*6*). The dependency of association kinetics on ionic strength has been repeatedly analyzed, and taken as an indication of the existence of long-range electrostatic forces (refs *7* and *8* and references therein). Temperature also modifies binding kinetics. Its influence has been quantified, in particular within the framework of thermodynamic measurements with a Biacore (for example, refs *9*−*12*). In addition, computational methods have been used to analyze the pH (*13*−*15*) or ionic strength (*16*−*18*) dependency of antigen−antibody binding. These three factors have thus been shown individually to influence kinetic rates. The specific aim of this work was to investigate their interdependency. In particular, electrostatic forces, which depend on molecular charges, are influenced by the pH and ionic strength of the buffer. These two factors may therefore act dependently on binding, while temperature is expected to influence binding in a manner that is independent of the two other factors.

The influence of various buffer conditions on antigen−antibody binding kinetics (*19*−*21*), including the cAbLys3−lysozyme interaction (*22*), was analyzed previously using a QSAR approach in which six factors were varied simultaneously. In these studies, the pH and NaCl concentration were varied at most within the ranges of 6.8−8.2 and 150−850 mM, respectively, and the relationship between kinetics and buffer properties was correctly described when including independent factor terms in the models. We have designed our experiments in such a way that interaction terms (dependency between factors) can be identified, and have chosen different pH and NaCl concentration ranges: 5−10 and 50−500 mM, respectively. The lowest NaCl concentration was decreased compared to that used in previous studies because substantial increases in k_{on} were recorded at NaCl concentrations of ≤100 mM (for a review, see ref *8*). The pH range of 5−10 was a compromise between scanning a wide pH region and retaining protein fold and activity. Temperature was varied in the range of 15−30 °C. The cAbLys3−lysozyme binding kinetics in multivariate buffers were assessed with a Biacore 2000 instrument (Biacore AB, Uppsala, Sweden). We have developed mathematical models relating kinetic parameters and environmental factors, and evaluated the predictive capacity of the models. Continuum electrostatic and titration calculations were performed on the crystallographic structures of the isolated and bound molecules, to propose a structural explanation for the observed effects.

MATERIALS AND METHODS

Surface Preparation for Biacore Experiments. Flow cell 1 (Fc1) of the CM5 sensor chips was used as reference surface; the other three flow cells were immobilized with low levels of antigen for kinetic measurements, or high levels for active concentration measurements. Lysozyme was immobilized using amine coupling chemistry (BiaApplications Handbook, Biacore AB). The flow rate was 10 μL/min. Surfaces for kinetic measurements were activated with 30 μL of EDC/NHS [*N*-ethyl-*N*′-(3-dimethylaminopropyl)-carbodiimide hydrochloride/*N*-hydroxysuccinimide, from Biacore AB]. Lysozyme, at 10 μg/mL in 10 mM NaH_2PO_4 (pH 8.0), was injected for 1−3 min, until the response reached 30−150 resonance units (RU). Surfaces for concentration measurements were activated with 100 μL of EDC/NHS, and lysozyme was injected for 5−10 min. The response level was >4000 RU. The surfaces were deactivated with 30 μL of ethanolamine-HCl, and washed with 10 μL of 50 mM HCl. Fc1 was treated like the kinetic surfaces except that no lysozyme was injected. In some experiments, the surfaces were activated by a 5 min injection of EDC/NHS and deactivated with ethanolamine before the immobilization procedure started, to neutralize the excess carboxyl groups of the dextran matrix. In another control experiment, biotinylated lysozyme (Biomeda E05) was immobilized on a streptavidin surface.

Kinetic Measurements with a Biacore. Buffers with pH's in the ranges of 5.5−6.5 and 8.5−9.5 were prepared with MES [2-(*N*-morpholino)ethanesulfonic acid] and TABS [*N*-tris(hydroxymethyl)methyl-4-aminobutanesulfonic acid], respectively. The buffer at pH 7.5 was prepared with HEPES [*N*-(2-hydroxyethyl)piperazine-*N*′-2-ethanesulfonic acid]. The buffers at pH 5.0 and 10.0 were prepared with MES and TABS, respectively, to prevent a change in the buffer ions. All buffers were at 10 mM, contained 0.005% P20 (Biacore) and 3.4 mM EDTA, and were degassed and filtered. The NaCl concentration varied between 50 and 500 mM, and the temperature for the measurements varied between 15 and 30 °C.

The analyte was a mutant of cAbLys3 (*23*) with the single D73R change remote from the interface with lysozyme, named cAbLys3-D73R, unpurified in cell supernatants. The mutant, available in large quantities, exhibited binding properties similar to those of the wild type (WT) in HEPES-buffered saline (HBS). Five 2-fold dilutions or three 3-fold dilutions of the analyte were prepared in the different buffers, starting from a solution adjusted to ∼50 nM in the same buffer. The injection and postinjection phases lasted between 2 and 3 min. The surfaces were regenerated with 50 mM HCl. Data were fitted globally with BIAevaluation 3.1 (Biacore AB), using the Langmuir or mass transfer limited models.

Active Concentration Measurements. The active concentrations of the cAbLys3-D73R preparations were measured at pH 7.5, 250 mM NaCl, and 25 °C, under conditions of total mass transport (*24*). The diluted samples were injected on a surface containing high levels of lysozyme, and the initial slope was recorded. A theoretical calibration curve relating the initial slope to the concentration of antibody fragments was established with the BIAsimulation software (Biacore AB), and was used to calculate the concentration of antibody fragments in the samples.

Statistical Analysis of Data. Data analysis was performed as described by Andersson et al. (*20*) and Choulier et al. (*21*). Briefly, the mathematical models were developed in MODDE 7.0 (Umetrics AB, Umeå, Sweden), using partial least squares (PLS) and the logarithm of k_{on} (log k_{on} values

are more normally distributed than the untransformed k_{on} values). In general, replicate data (between two and four measurements under each experimental condition) were entered separately. In some cases, the modeling was repeated using mean instead of replicate values to assess the robustness of the models. The quality of the models was estimated using R^2 (percent of variation of the response explained by the model) and Q^2 (leave-one-out cross-validation). In screening experiments, individual terms (pH, NaCl concentration, and temperature) and interaction terms (temperature × pH, temperature × NaCl concentration, and pH × NaCl concentration) were initially included in the models. For response surface modeling, quadratic terms (pH × pH, NaCl concentration × NaCl concentration, and temperature × temperature) were added. Non significant terms were removed to maximize Q^2 and R^2. Models were considered acceptable for $Q^2 > 0.6$.

Molecular Modeling. Continuum electrostatics calculations were performed to determine the total charge of the antibody−lysozyme complex, as well as isolated antibody (cAbLys3) and lysozyme as a function of pH. Several experimental structures of cAbLys3−lysozyme complexes are available. To check the internal consistency of the results, we performed calculations on Protein Data Bank (PDB) entry 1MEL (*2*) (where we used the complex labeled AL in the PDB entry) and PDB entry 1JTT (*1*). For PDB entry 1MEL, we kept the original amino acid sequence of the antibody. For PDB entry 1JTT, we introduced the point mutation that corresponds to the sequence used in the Biacore experiments (D73R). The side chain of the mutated amino acid was placed with SCWRL (*25*), using the structure of the wild-type 1JTT complex as a starting point. The hydrogen atoms were added using the HBUILD facility of CHARMM (*26*), and the structures were minimized using 1000 steps of steepest descent followed by 1000 steps of the adopted basis Newton−Raphson method. In experimental structure 1JTT, two alternative conformations of His 111 of cAbLys3, which is situated at the protein−protein interface, are found. Two structure files (one with each orientation) of the cAbLys3-D73R mutant were therefore constructed and used in the pK_a calculations. For other amino acids with multiple occupancies, the most populated conformation was selected. In the absence of an experimental structure for the isolated antibody, the structures used in the pK_a calculations of the isolated proteins were taken from the PDB file of the complex. The use of several experimental structures (1MEL and 1JTT A and B) nevertheless allows the assessment of the sensitivity of the procedure to small structural variations.

Titration calculations for the complex and isolated cAbLys3 and lysozyme were performed as described in refs *27* and *28* using shell scripts developed by M. Schaefer (personal communication), and UHBD (*29*) for continuum electrostatic calculations. The dielectric constant used for the protein was 20 and for the solvent 80. A choice of 20 for the internal dielectric constant has been shown to give calculated pK_a values consistent with experimental data (*30*). Tests performed using values of 4 and 8 for the internal dielectric constant showed that using different values of the protein dielectric constant would not affect the conclusions of the pK_a calculations. The final focusing grid around the titratable sites had a spacing of 0.3 Å. Global titrations of the complex, isolated cAbLys3, and isolated lysozyme (including all Lys, Arg, Glu, Asp, His, and Tyr residues) were performed using a Monte Carlo procedure (*31*). This yields 61 titratable sites for the complex: 31 for cAbLys3 and 30 for lysozyme. On structure 1MEL, titrations were also performed for a reduced number of sites at the interface between cAbLys3 and lysozyme, using an exact titration method (*27*). The His residues situated at the cAbLys3−lysozyme interface and all Asp, Arg, Glu, and Lys residues situated within 15 Å of these histidines, as well as the N- and C-terminal ends, are titrated. This yields 21 sites for the complex: 9 for lysozyme and 12 for cAbLys3. A smaller titration set comprising only the local interface residues (Asp 99, Glu 108, and His 111 for cAbLys3 and Arg 112 for lysozyme) was also tested. The titration curves were calculated for two ionic strength values, 50 and 500 mM.

RESULTS

Experimental Design. Two sets of experiments were designed. The first set (named set 1) consisted of a screening in the pH range of 6.0−9.0 for identification of factors which influence binding and investigation of the existence of a dependency between factors. These questions were answered using a full factorial design at two levels, which requires binding kinetics to be measured in nine conditions of the experimental region, represented as circles in Figure 1A. In this first set of experiments, the NaCl concentration, pH, and temperature ranges were 50−500 mM, 6−9, and 20−30 °C, respectively (Figure 1B).

The second set (named set 2) consisted of a response surface modeling (RSM) analysis that allows a more detailed modeling. The design that was used (full factorial design at three levels) can support quadratic terms and requires kinetic parameters to be measured under 18 additional conditions compared to the screening design (squares in Figure 1A). The aim of the set 2 experiments was not only to confirm and/or refine the mathematical models deduced from screening but also to investigate whether similar models can be developed from different pH regions and to evaluate the ability of these models to predict kinetic parameters over a wide pH range. The NaCl, pH, and temperature ranges were 100−400 mM, 5.0−10.0, and 15−25 °C, respectively (Figure 1C). The NaCl and temperature ranges were slightly shifted compared to those in set 1 to facilitate data evaluation (see below). The design of set 2 thus included the analysis of kinetic parameters under 81 conditions: at nine pH values, at three NaCl concentrations, and at three temperatures. Each measurement was performed at least twice.

Quality of the Kinetic Data. The rate of association of the cAbLys3-D73R−lysozyme interaction was substantially faster at pH ≤6.0 and ≤100 mM NaCl than under other experimental conditions, leading in some cases to partial mass transport. Panels A and B of Figure 2 show typical sensorgrams obtained at pH 6.0 and 20 °C, in either 50 or 500 mM NaCl, clearly illustrating the faster association at low (Figure 2B) than at high (Figure 2A) salt concentrations, and the lower quality of the fits in the former case, even when using the mass transport limited model. The fitted R_{max} value (maximal binding capacity of the sensor surfaces) was typically between 85 and 115% of that at pH 7.5 and 250 mM NaCl, except at pH 5.0 where the fitted R_{max} tended to be larger. Standard deviations for kinetic rate parameters at

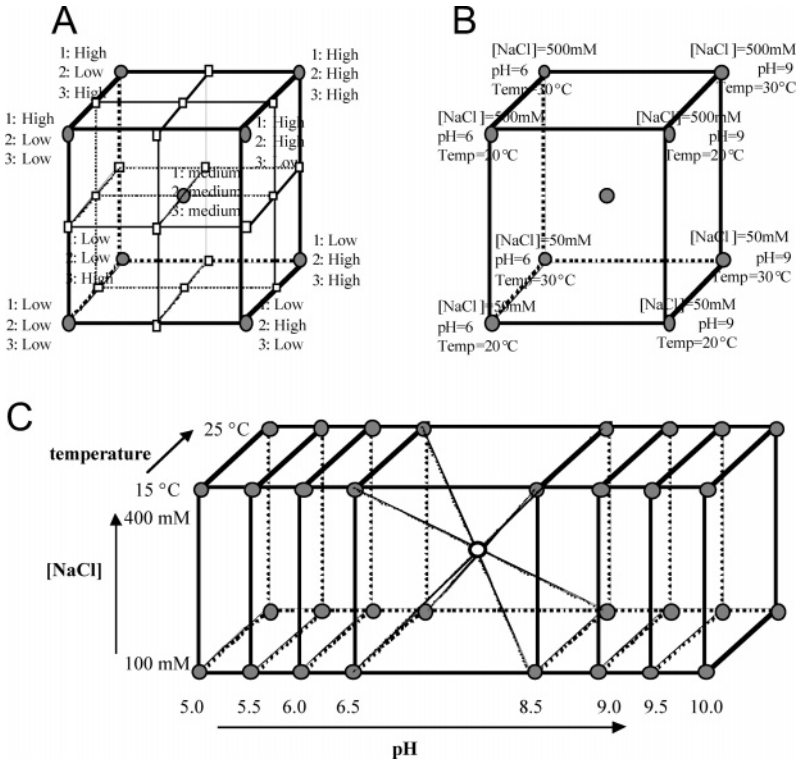

FIGURE 1: Multivariate experimental design. (A) Experimental region and designs for three factors, 1−3. The nine multivariate conditions analyzed for screening are represented by gray spheres. The 18 additional conditions analyzed for RSM are represented by white squares. (B) Experimental region and conditions (gray spheres) in set 1. (C) Experimental region and screening conditions in set 2. The RSM conditions are not represented.

pH ≤5.5 were up to 70%. Data at pH ≥6.0 were of good quality with X_2 values of typically less than 5% of the R_{max} and standard deviations on mean k_{on} and k_{off} values calculated from independent experiments of mostly less than 20%. Kinetic measurements at low salt concentrations and pH were reproduced on surfaces where biotinylated lysozyme was captured on streptavidin, indicating that kinetic data were not influenced by surface properties.

Kinetic Parameter Variations. The smallest and largest mean k_{on} values when combining data from sets 1 and 2 were 5×10^4 M^{-1} s^{-1} (pH 9.5, 100 mM NaCl, 15 °C) and 2×10^7 M^{-1} s^{-1} (pH 6.0, 50 mM NaCl, 30 °C), respectively, resulting in a 400-fold variation over the experimental regions that were analyzed. The smallest and largest mean k_{off} values were 5×10^{-4} s^{-1} (pH 9.5, 400 mM NaCl, 15 °C) and 8×10^{-3} s^{-1} (pH 5.0, 100 mM NaCl, 20 °C), respectively, resulting in a 16-fold variation. In set 1, the k_{on} and k_{off} variations were 79- and 4-fold, respectively, and in set 2, they were 154- and 16-fold, respectively. The pH and NaCl concentration sensitivities of the kinetic rates are illustrated in Figure 2C for data obtained at 20 °C (set 2): the mean values for the kinetic parameters are expressed in % relative to the value at pH 7.5, 20 °C, and 250 mM NaCl (central point of the experimental region). The k_{on} (gray bars) increases at pH <6.0. The magnitude of this increase depends on the salt concentration, indicating a dependency between NaCl concentration and pH for their effect on k_{on}. The k_{off} (white bars) shows a low sensitivity to pH and NaCl concentration with a slight increase at extreme pH values. Similar patterns of changes were observed at 15 and 25 °C (data not shown), with kinetic parameters increasing with temperature. The QSAR modeling will focus on k_{on} variations.

QSAR Modeling from Screening. Mathematical models that relate variations of k_{on} with variations in buffer conditions were first developed from set 1 data. Statistical parameters were slightly better when entering replicate k_{on} values ($Q^2 = 0.84$ and $R^2 = 0.95$) rather than the mean ($Q^2 = 0.71$ and $R^2 = 0.85$). Both models included the terms pH, NaCl, and pH × NaCl, and indicated that pH × temperature and NaCl × temperature terms do not influence the on-rates (data not shown). Temperature is identified when using replicate, but not mean, k_{on} values. This uncertainty may be due to the low quality of data recorded under conditions of partial mass transport, which is favored at low salt concentrations and high temperatures. The second set of experiments (set 2) was therefore conducted in slightly shifted NaCl concentration (100−400 mM instead of 50−500 mM) and temperature (15−25 °C instead of 20−30 °C) ranges (see Figure 1B,C) to facilitate data evaluation. The set 2 data, which included the nine conditions required for screening, were first used to derive new screening models in the pH range of 6−9. The models confirm the influence on k_{on} of pH, NaCl, pH × NaCl, and temperature (Figure 3A). Statistical parameters are good ($Q^2 > 0.6$ and $R^2 > 0.8$) whether using replicate or mean k_{on} values. Furthermore, a screening model developed from a slightly wider pH range (5.5−9.5 instead of 6.0−9.0) was similar (Figure 3A).

Response Surface Modeling. Next we investigated whether the models could be refined by response surface modeling (RSM), using 27 data points as represented in Figure 1A. RSM in the pH ranges of 5.5−9.5 and 6.0−9.0 confirmed the conclusions from screening and identified the pH × pH term as an additional term (Figure 3B). The pH × temperature and NaCl concentration × NaCl concentration terms showed only a minor contribution, and were not identified

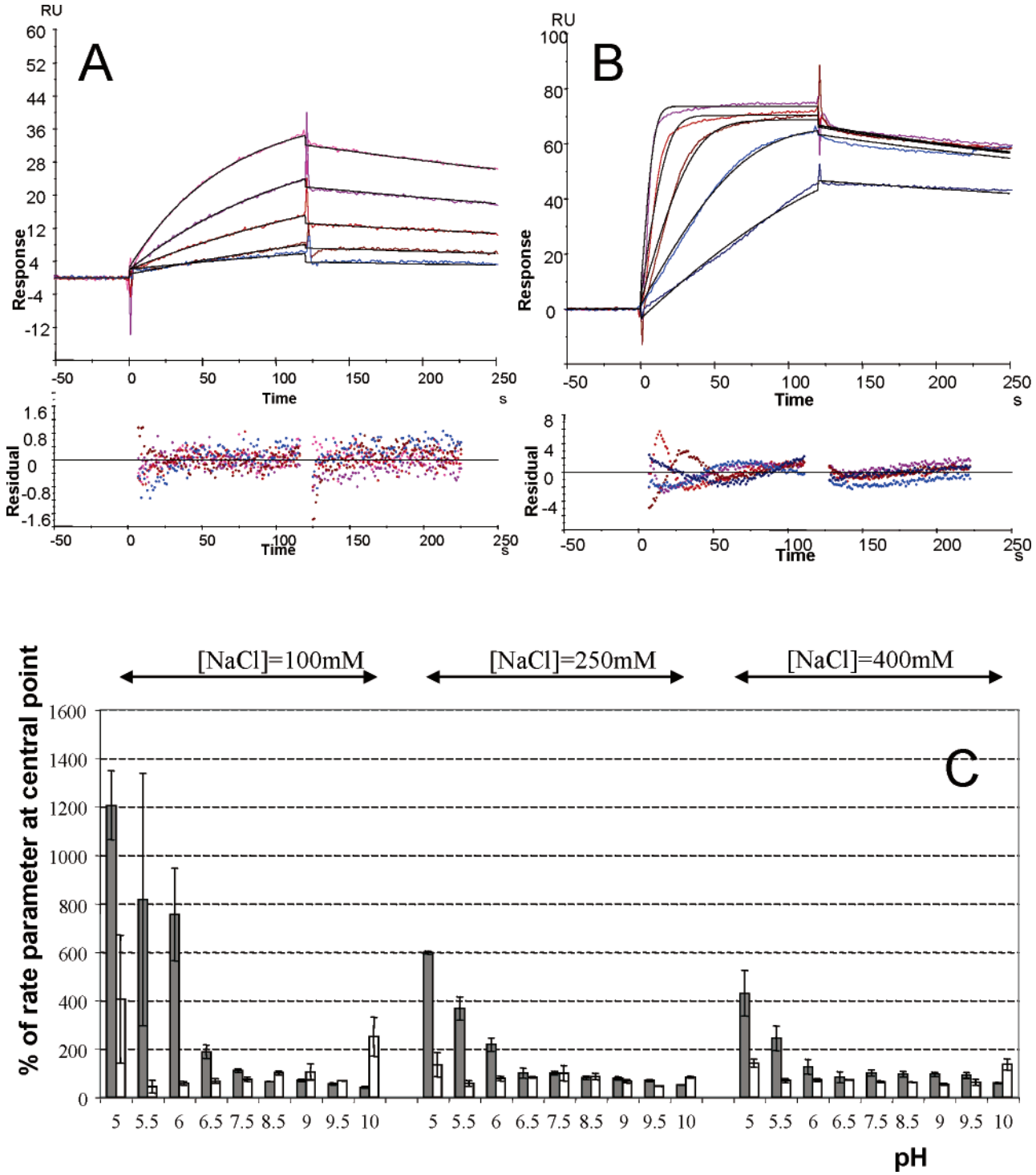

FIGURE 2: Influence of pH and salt on kinetic rate parameters. (A and B) Typical sets of sensorgrams corresponding to the injection of five concentrations of cAbLys3-D73R (from 3 to 48 nM) on a lysozyme surface at pH 6.0 and 20 °C in (A) 500 mM NaCl and (B) 50 mM NaCl: experimental (colored) and fitted (black) curves, using the Langmuir (A) and the mass transfer limiting (B) models. (C) Variations of k_{on} (gray bars) and k_{off} (white bars) as a function of pH and NaCl concentration at 20 °C. Rate parameters are expressed in percent relative to the value at pH 7.5, 20 °C, and 250 mM NaCl (central point in Figure 1C). Error bars represent the standard deviation of the mean of two to four experiments.

with data from both pH ranges. The statistical parameters of the RSM models were not significantly better than those of the screening models.

Validation of the Models from Predictions. The validity of the mathematical models was evaluated from their predictive capacity over all pH ranges, namely within the pH region used to develop the model, or at higher and lower pH's. Panels C and D of Figure 3 show plots of observed versus predicted log k_{on} calculated from the screening and RSM models developed in the pH range of 6−9. The four groups of data points correspond to the learning set (black), other values available in the pH range of 6−9 (test set, blue), values at pH <6.0 (green), and values at pH >9.0 (red). The models developed in the pH range of 5.5−9.5 have similar predictive capacities (data not shown). Regardless of the model, residuals are <0.1 in the pH region used to develop

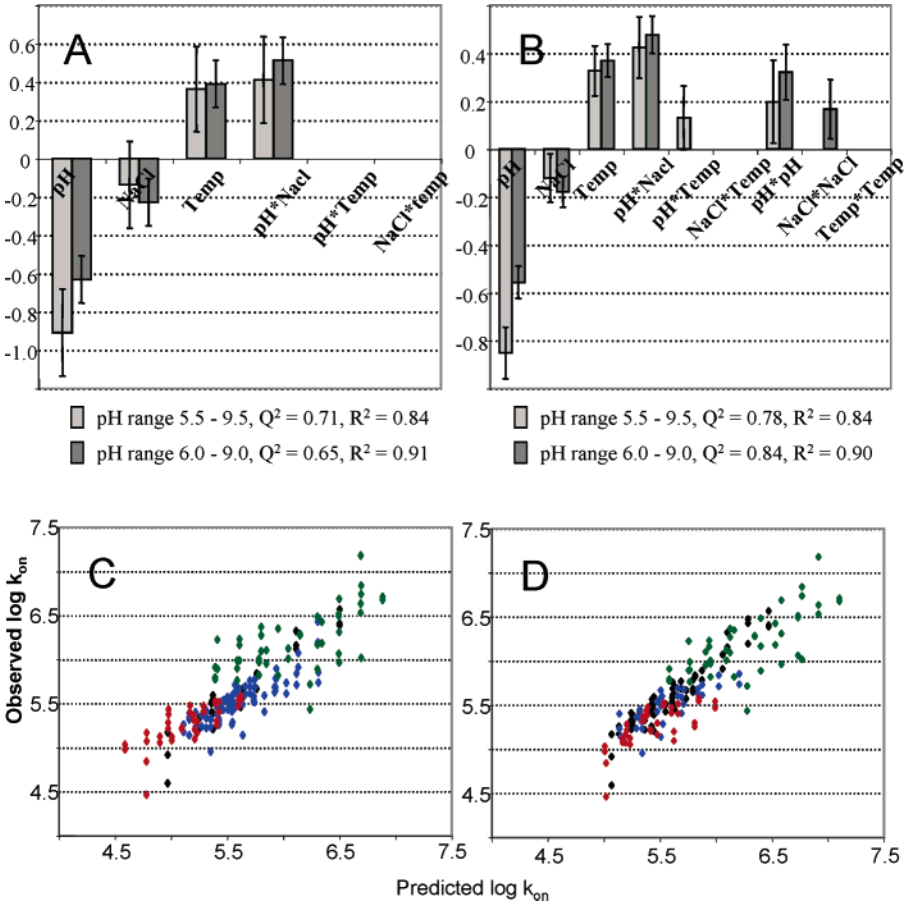

FIGURE 3: Comparison of the screening (A and C) and RSM (B and D) models. (A and B) Histogram representation of the effects (*46*) identified from screening and RSM, respectively, in the pH ranges of 5.5−9.5 (light gray) and 6.0−9.0 (dark gray). The effect represents the change in log k_{on} when the corresponding factor is varied from the low to the high level (other factors being kept at the central value). Error bars represent the 95% confidence interval. (C and D) Predictive capacity of the screening and RSM models, respectively, developed in the pH range of 6.0−9.0. Plots of predicted vs observed log k_{on} for the training set (black), other data in the pH range of 6.0−9.0 (blue), and data recorded at pH <6.0 (green), and pH >9.0 (red).

the model and <0.18 in other pH ranges. Residuals for set 1 data are <0.1 when excluding data recorded at 50 mM NaCl. We thus demonstrate that the screening models are sufficient to correctly describe the relationship between factors and on-rates, and that these models can predict k_{on} not only in the region covered by the experimental design but also outside this region.

Molecular Modeling. The full titration of the lysozyme and cAbLys3 showed that the total charge of the isolated lysozyme diminishes when pH increases, with a calculated isoelectric point for lysozyme of 11.4, which is in good agreement with the experimental value of 11.2 (*32*) (Figure 4). For cAbLys3-D73R, the isoelectric point is estimated to be at a pH of 5.6 (Figure 4). The two titration curves run parallel to each other in the pH range of 6−12 so that the difference between the net charge of lysozyme and cAbLys3 remains stable at ∼8 *e* for a large pH range, with the lysozyme positively and the cAbLys3 negatively charged. This behavior is observed with both structures (PDB entries 1JTT and 1MEL) and with both titration methods. Thus, there are no large changes in the relative charges of the lysozyme and cAbLys3 in the pH range of 6−12. At pH <6, the titration of cAbLys3 reduces the charge difference between the two proteins, and the cAbLys3 becomes positively charged. The comparison of the results for the mutant D73R and wild-type antibody shows that the D73R mutation has some influence on the isoelectric point of cAbLys3, but does not influence the overall characteristics of the titration, or the titration behavior of the amino acids situated at the protein−protein interface, as residue 73 is solvent-exposed and remote from the interface.

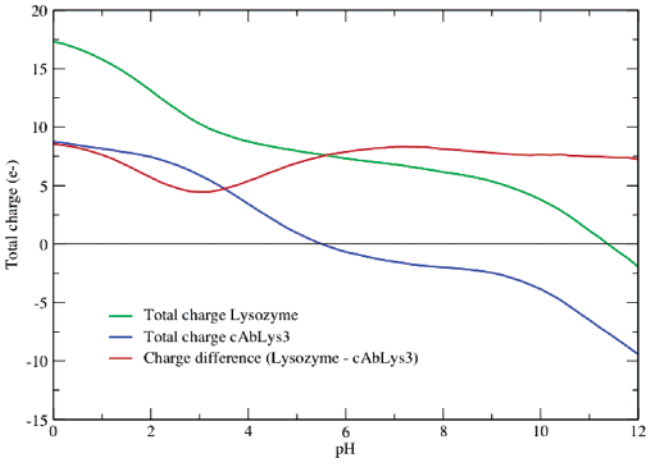

FIGURE 4: Total charge of lysozyme and cAbLys3-D73R as a function of pH, as well as the difference between the total charges of lysozyme and cAbLys3. Data were obtained using PDB entry 1JTT and the Monte Carlo titration procedure (see the text for details). Data obtained using 1MEL complexes or reduced titration methods show similar relative values of the charges as a function of pH (data not shown).

Table 1: Calculated pK_a Values for His 111 of cAbLys3 in Complex with Lysozyme, and cAbLys3 Isolated[a]

structure	ionic strength (mM)	pK_a (complex)	pK_a (cAbLys3)	Δ (complex-free)
1MEL[b]	50	5.6[d]	6.6	−1.0
1JTT A[c]	50	6.6	6.9[e]	−0.3
1JTT B[c]	50	6.1	6.9[e]	−0.8
1MEL[b]	500	5.6	6.5	−0.9
1JTT A[c]	500	6.6	6.7	−0.1
1JTT B[c]	500	6.1	6.7	−0.6

[a] Data obtained by full titration (see the text for details). The reference (solution) pK_a used for histidines in the pK_a calculations is 6.42 (*45*). [b] Identical (to the first decimal) values for the pK_a of His 111 in 1MEL were obtained when using the exact titration with a reduced number of sites and the Monte Carlo method with full titration (see Materials and Methods for details). [c] His 111 has different orientations in 1JTT A and 1JTT B from the experimental crystal structure. The D73R replacement was introduced into 1JTT A and B prior to pK_a calculations. [d] In 1MEL, His 111 points toward Arg 112 of lysozyme. If the charges of Arg 112 are set at zero, the pK_a of His 111 increases to 6.6 in the 1MEL complex. [e] His 111 makes favorable interactions with Glu 108 (distance 3.5 Å) and Asp 99 (distance 7 Å) in 1JTT A and B, respectively. This explains its similar pK_a calculated for these two conformations in free cAbLys3. If the charges of Glu 108 are set to zero in the isolated 1JTT A, the pK_a of His 111 becomes 6.0, while if the charges of Asp 99 are set to zero in the isolated 1JTT B, the pK_a of His 111 becomes 6.2 (it must be noted that Glu 108 is solvent-exposed, while Asp 99 is buried, and that their influence is linked to their distance from His 111 and to the local dielectric environment).

The pK_a calculations also identify the titratable groups situated at the protein−protein interface that could change the pK_a values upon formation of the complex, as well as the interfacial residues that change protonation in the pH range of the experimental measurements. The individual titration curves of the amino acids in the complex and isolated proteins showed that acidic amino acids tended to have lower pK_a values and basic amino acids higher pK_a values in the protein environment relative to their value in solution (data not shown). Thus, the modification of the dielectric environment does not yield unexpected titration behaviors for Asp, Glu, Lys, and Arg residues, and these residues do not change protonation state in the range of pH around 6.0 where experimental effects are observed.

The only amino acid that changes protonation state in the range of pH around 6.0 where experimental effects are observed, and that is sensitive to the formation of the complex, is His 111 from cAbLys3 (Table 1). In the free antibody, the pK_a of His 111 is somewhat higher than for a free His in solution, which can be understood by the proximity of acidic amino acids of the antibody (Glu 108 and Asp 99), which tend to stabilize the positively charged form of His 111 and therefore increase its pK_a somewhat. In the absence of an experimental structure, the three structures used for the free antibody were taken from the complexes. The results for the three structures of the free antibody are, however, reasonably similar. The pK_a values of His 111 in the complex differ for the three structures that were used (Table 1). Comparison of the results shows that in PDB entries 1MEL and 1JTT B, His 111 has a lower pK_a in the complex than in the free antibody, while in PDB entry 1JTT A, complexation does not influence the pK_a of His 111 much. These differences are linked to different electrostatic interactions with nearby charged amino acids, namely, Glu 108 and Asp 99 of cAbLys3 itself and Arg 112 of lysozyme (see Figure 5). Indeed, in the X-ray structures, His 111 adopts two alternate positions with different local environments. In 1MEL and 1JTT B, His 111 electrostatically interacts with Arg 112 of lysozyme (distance of ∼5−6 Å in 1JTT B and 4−5 Å in 1MEL). As a result, the positively charged form of His 111 is destabilized, and its pK_a is lowered in the complex. In 1JTT A, on the other hand, His 111 is close to Glu 108 of cAbLys3 (distance of ∼3.5 Å) and farther from Arg 112 of lysozyme (distance of ∼9 Å). As a result, the pK_a of His 111 in this structure is somewhat higher than for a free His. The fact that the titration behavior of His 111 is influenced mainly by the three charged amino acids, Glu 108, Asp 99 (cAbLys3), and Arg 112 (lysozyme), was verified by repeating the titration calculation with the charges for the side chain of these amino acids set to zero (see the footnote of Table 1). This confirmed that the differences in calculated pK_a values between the different complexes are linked to differences in the geometry of the interface around His 111 and, in particular, the relative positions of Asp 99, Glu 108, and Arg 112.

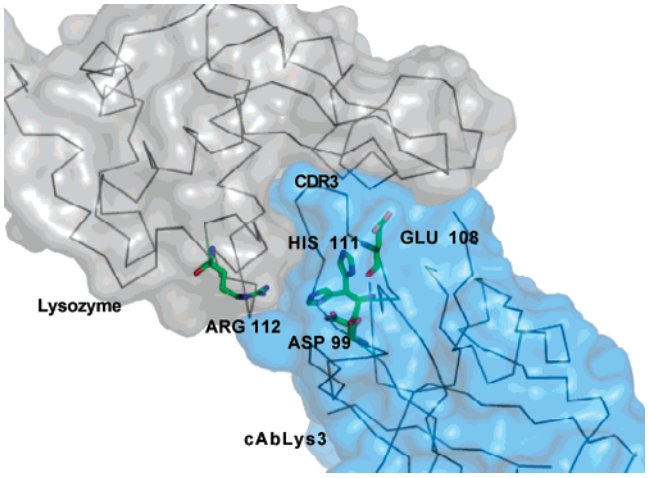

FIGURE 5: Interface of the cAbLys3 (blue)−lysozyme (gray) complex from 1JTT. The two orientations of His 111 are shown, as well as residues Asp 99 and Glu 108 from cAbLys3 and residue Arg 112 from lysozyme. The CDR3 of cAbLys3 that protrudes into the lysozyme active site is indicated. See the text for details.

Finally, the calculations indicate that in the free antibody, the ionic strength has a weak influence on the pK_a values of His 111 and Glu 108, which are situated at the surface of the cAbLys3. However, in the complex, ionic strength does not influence the pK_a as the amino acids are more buried (Table 1).

DISCUSSION

Importance of a Multivariate Approach. The multivariate QSAR approach that we applied was informative in two aspects of this study. First, the effect of pH and NaCl concentration on association kinetics would have been overlooked in a single perturbation analysis in which either the NaCl concentration or pH is varied, starting from standard conditions (pH >6.5, [NaCl] > 100 mM). Indeed, the influence of salt on k_{on} is only apparent at pH ≤6.5: when the NaCl concentration is decreased from 400 to 100 mM at 20 °C, the k_{on} increases by a factor of 6.5 at pH 6.0 and by a factor of 1.2 only at pH 7.5. Conversely, the influence of pH on k_{on} is most apparent at NaCl concentrations of ≤100 mM: when the pH is decreased from 9.0 to 6.0 at 20 °C,

the k_{on} increases by a factor of 10 at 100 mM NaCl but by a factor of 2.8 only at 250 mM NaCl. The multivariate QSAR approach, in which factors are varied simultaneously, thus demonstrated a dependency between NaCl concentration and pH for their effect on k_{on}, which allowed us to identify the influence of these factors on binding.

The second advantage of the multivariate approach was the predictive potential of the mathematical models that relate k_{on} with experimental conditions. The RSM approach, which requires binding kinetics to be measured in 27 experimental conditions, did not significantly improve the statistical parameters of the models, or their predictive capacity, compared to the screening models (Figures 3). Our results thus show that the three factors analyzed (pH, NaCl concentration, and temperature) influence the on-rate of the cAbLys3-D73R−lysozyme interaction in a complex way that can be modeled from a limited number of experiments (kinetic measurements under nine conditions). Furthermore, similar models were obtained when using kinetic parameters obtained at pH 5.5 and 9.5, instead of pH 6.0 and 9.0 (Figure 3A,B), despite the lower quality of the data at pH 5.5 and 100 mM NaCl (Figure 2C).

The observation that small but concomitant changes in simple environmental factors may significantly modify molecular binding properties has important practical implications. The behavior of a binder in vivo or in harsh environments may greatly differ from its behavior in a standard buffer. The practical applicability of assays developed under standard laboratory conditions is often limited (*33*). In particular, the reliability of quantifications may be questioned if changes in pH or the presence of additives may alter binding affinity. Simple QSAR experiments can be used to optimize kinetic parameters for biotechnological applications, or to predict binding parameters under conditions that cannot be adjusted.

Relationship among Structure, Environment, and Binding. We have shown that the kinetics of binding of the single-domain antibody cAbLys3 to hen egg white lysozyme are affected by pH and ionic strength, with the larger effect being on the association rate parameter. Whereas the dissociation rate depends on short-range interactions formed in the complex, the association rate is controlled by their diffusion and the geometrical constraints of the binding sites (*34*, *35*). Theoretical and experimental studies have shown that the rate of association between large molecules of opposite charges can be accelerated by the so-called electrostatic steering effect, leading to k_{on} values on the order of 10^8−10^{10} M^{-1} s^{-1}, as compared to values of 10^5−10^6 M^{-1} s^{-1} for association controlled by rotational and translational diffusion (refs *7* and *8* and references therein). Experimental indications for electrostatic steering are a dependency of k_{on} on ionic strength and the absence of an effect of ionic strength on k_{off} (*34*). These two phenomena are not observed in our system at neutral pH, but become apparent at pH ≤6.5.

Although our experimental data clearly suggest a role for electrostatic interactions in binding kinetics, they do not fit the classical electrostatic steering explanation. A first observation is that the on-rates are slow with respect to typical examples of electrostatically driven association. The highest measured on-rate for the cAbLys3-D73R−lysozyme interaction (2×10^7 M^{-1} s^{-1} at pH 6.0, 30 °C, and 50 mM NaCl) is at least 1 order of magnitude lower than those observed for molecules displaying charge complementarity, such as colicin E3/immunity protein 3 (*34*, *36*) or barnase/barstar (*7*). Furthermore, while the overall variation in on-rate can be substantial (154-fold in set 2), the influence of ionic strength on the on-rate of the cAbLys3-D73R−lysozyme interaction at a given temperature and pH is relatively small (maximum of 17-fold, when the NaCl concentration decreases from 500 to 50 mM at pH 6.0 and 30 °C). Thus (and although some caution must be exercised when comparing studies where different salt concentrations and measurement methods were used), the magnitude and sensitivity to ionic strength of the association rate for the cAbLys3-D73R−lysozyme interaction appear globally to be more similar to what has been observed in systems where electrostatic steering was not considered important (*5*, *37*, *38*). Finally, the fact that the fastest association is observed at low pH cannot be easily reconciled with a simple view of electrostatic steering since the titration curves of cAbLys3 and lysozyme (Figure 4) show that lysozyme is positively charged and cAbLys3 negatively charged in the pH range of 6−10. Furthermore, as the isoelectric point of cAbLys3-D73R is ∼6, decreasing the pH decreases the difference in charge between the two associating proteins, and at low pH, cAbLys3 becomes positively charged like the lysozyme.

Huang and Briggs (*39*) have observed electrostatically accelerated association between two negatively charged molecules, and have shown by modeling that a local patch of positive charges situated at the binding pocket of one of the proteins was contributing to electrostatic steering, even though the protein was globally negatively charged. Local electrostatic steering could be imagined if, for example, histidines were facing acidic amino acids in the protein interface. In that event, lowering the pH below the pK_a of the histidines while keeping it above the pK_a of the acidic group could locally enhance electrostatic interactions. In our particular case, the protein−protein complex contains two His residues and only one (His 111 from cAbLys3) is situated at the protein−protein interface. There are, however, no acidic amino acids from lysozyme within 10 Å of His 111 (cAbLys3); the only titratable group of lysozyme within 10 Å of His 111 is Arg 112 (Figure 5). Thus, local electrostatic steering effects do not appear to be likely in our particular system.

Phenomena that are alternatives to electrostatic steering must be responsible for the k_{on} variations that we observe. The possibility of a nonspecific attraction between the antibody fragment used as an analyte and the negatively charged dextran matrix can be excluded because no binding is observed on the control surface; furthermore, the data were reproduced on a surface that had been activated or deactivated prior to lysozyme immobilization to neutralize excess carboxyl groups, and also on a streptavidin−biotinylated lysozyme surface. Moreover, these control experiments exclude the possibility of pH-dependent electrostatic interaction effects between the immobilized molecules and the dextran matrix (*40*), which could influence lysozyme−antibody binding.

The experimentally observed pH dependency of the association rate suggests a role for His 111, as it is the only amino acid of the interface that titrates in the pH range (around 6.5) where the kinetics are affected. The titration behavior of His 111 was confirmed by the continuum

electrostatic calculations that explicitly consider the environment of charged residues in the protein−protein complex. That such interactions can have a significant influence on pK_a values has been demonstrated in several studies (*14*, *15*, *41*), so interpreting pH effects solely on the basis of solution pK_a values can be misleading. Our titrations showed that in the free cAbLys3, the pK_a of His 111 is somewhat higher than that in solution, while complex formation is accompanied by a lowering of its pK_a, particularly when His 111 points toward Arg 112 of lysozyme. Two negatively charged amino acids of cAbLys3 itself are within 10 Å of His 111: Asp 99 and Glu 108, which are situated in the N- and C-terminal ends of the CDR3 of cAbLys3. This hypervariable loop of the antibody inserts deeply into the binding pocket of lysozyme and makes the most significant contributions to binding in this protein−protein complex (*23*, *42*, *43*). Asp 99, Glu 108, and His 111 themselves do not form important energetic interactions with lysozyme (*43*), which is consistent with the experimental observation that pH does not influence much the dissociation rate parameter of the complex. They are, however, sufficiently close to the interface to exhibit small changes in surface area upon binding. A tentative explanation for the rate enhancement at low pH (when His is positively charged) is the occurrence of stronger intramolecular interactions between His 111 and Glu 108 that stabilize a conformation of cAbLys3 that associates faster with lysozyme. For example, Glu 108 together with a positively charged nearby His 111 could act as a globally neutral group that would be more easily desolvated in the early stages of binding. Conformational entropy effects in the formation of a rate-limiting transition state for binding could also be at play. It must be noted that in a separate QSAR study by other authors (*44*), the conformation of His 111 had been mentioned as one of the factors that influence k_{on} values. These conclusions were based, however, on a totally different reasoning, using molecular models of cAbLys3 mutants at positions 101 and 105 for which antigen binding kinetics had been measured (*22*). Clearly, more detailed calculations of the kinetics of association would be needed to obtain a complete mechanistic interpretation of the interplay between the His 111 charge, its interactions with Glu 108 and Asp 99 of cAbLys3 and Arg 112 of lysozyme, and the link between these interactions, the conformation, solvation, and the flexibility of the CDR3 loop and the kinetics of binding. These detailed calculations are beyond the scope of this work. The current experimental data clearly show that substantial modification of association kinetics can be observed when the pH and NaCl concentration are changed, with a clear dependency between these two factors. The continuum electrostatic calculations show that these effects cannot be explained by simple models of electrostatic steering and that more subtle effects are at play. Together, the experimental and computational data provide additional insight into the complex mechanisms of protein−protein association.

ACKNOWLEDGMENT

We thank K. Andersson and R. Stote for critical reading of the manuscript.

SUPPORTING INFORMATION AVAILABLE

Main effects identified from screening in the pH range of 6−9, shown as the mean and standard deviation on residuals for observed versus predicted log k_{on} values calculated from four models. This material is available free of charge via the Internet at http://pubs.acs.org.

REFERENCES

1. Decanniere, K., Transue, T. R., Desmyter, A., Maes, D., Muyldermans, S., and Wyns, L. (2001) Degenerate interfaces in antigen−antibody complexes, *J. Mol. Biol. 313*, 473−8.
2. Desmyter, A., Decanniere, K., Muyldermans, S., and Wyns, L. (2001) Antigen specificity and high affinity binding provided by one single loop of a camel single-domain antibody, *J. Biol. Chem. 276*, 26285−90.
3. Shen, B. J., Hage, T., and Sebald, W. (1996) Global and local determinants for the kinetics of interleukin-4/interleukin-4 receptor α chain interaction. A biosensor study employing recombinant interleukin-4-binding protein, *Eur. J. Biochem. 240*, 252−61.
4. Gossas, T., and Danielson, U. H. (2003) Analysis of the pH-dependencies of the association and dissociation kinetics of HIV-1 protease inhibitors, *J. Mol. Recognit. 16*, 203−12.
5. Piehler, J., and Schreiber, G. (1999) Biophysical analysis of the interaction of human ifnar2 expressed in *E. coli* with IFNα2, *J. Mol. Biol. 289*, 57−67.
6. Hugo, N., Lafont, V., Beukes, M., and Altschuh, D. (2002) Functional aspects of co-variant surface charges in an antibody fragment, *Protein Sci. 11*, 2697−705.
7. Schreiber, G., and Fersht, A. R. (1996) Rapid, electrostatically assisted association of proteins, *Nat. Struct. Biol. 3*, 427−31.
8. Zhou, H. X. (2003) Association and dissociation kinetics of colicin E3 and immunity protein 3: Convergence of theory and experiment, *Protein Sci. 12*, 2379−82.
9. Roos, H., Karlsson, R., Nilshans, H., and Persson, A. (1998) Thermodynamic analysis of protein interactions with biosensor technology, *J. Mol. Recognit. 11*, 204−10.
10. Day, Y. S., Baird, C. L., Rich, R. L., and Myszka, D. G. (2002) Direct comparison of binding equilibrium, thermodynamic, and rate constants determined by surface- and solution-based biophysical methods, *Protein Sci. 11*, 1017−25.
11. Deinum, J., Gustavsson, L., Gyzander, E., Kullman-Magnusson, M., Edstrom, A., and Karlsson, R. (2002) A thermodynamic characterization of the binding of thrombin inhibitors to human thrombin, combining biosensor technology, stopped-flow spectrophotometry, and microcalorimetry, *Anal. Biochem. 300*, 152−62.
12. De Genst, E., Handelberg, F., Van Meirhaeghe, A., Vynck, S., Loris, R., Wyns, L., and Muyldermans, S. (2004) Chemical basis for the affinity maturation of a camel single domain antibody, *J. Biol. Chem. 279*, 53593−601.
13. Gibas, C. J., Subramaniam, S., McCammon, J. A., Braden, B. C., and Poljak, R. J. (1997) pH dependence of antibody/lysozyme complexation, *Biochemistry 36*, 15599−614.
14. Livesay, D., Linthicum, S., and Subramaniam, S. (1999) pH dependence of antibody:hapten association, *Mol. Immunol. 36*, 397−410.
15. Gibas, C. J., Jambeck, P., and Subramaniam, S. (2000) Continuum electrostatic methods applied to pH-dependent properties of antibody−antigen association, *Methods 20*, 292−309.
16. Kozack, R. E., d'Mello, M. J., and Subramaniam, S. (1995) Computer modeling of electrostatic steering and orientational effects in antibody−antigen association, *Biophys. J. 68*, 807−14.
17. McDonald, S. M., Willson, R. C., and McCammon, J. A. (1995) Determination of the pK_a values of titratable groups of an antigen−antibody complex, HyHEL-5-hen egg lysozyme, *Protein Eng. 8*, 915−24.
18. Slagle, S. P., Kozack, R. E., and Subramaniam, S. (1994) Role of electrostatics in antibody−antigen association: Anti-hen egg lysozyme/lysozyme complex (HyHEL-5/HEL), *J. Biomol. Struct. Dyn. 12*, 439−56.
19. Andersson, K., Gulich, S., Hamalainen, M., Nygren, P. A., Hober, S., and Malmqvist, M. (1999) Kinetic characterization of the interaction of the Z-fragment of protein A with mouse-IgG3 in a volume in chemical space, *Proteins 37*, 494−8.

20. Andersson, K., Choulier, L., Hamalainen, M. D., van Regenmortel, M. H., Altschuh, D., and Malmqvist, M. (2001) Predicting the kinetics of peptide-antibody interactions using a multivariate experimental design of sequence and chemical space, *J. Mol. Recognit. 14*, 62−71.
21. Choulier, L., Andersson, K., Hamalainen, M. D., van Regenmortel, M. H., Malmqvist, M., and Altschuh, D. (2002) QSAR studies applied to the prediction of antigen−antibody interaction kinetics as measured by BIACORE, *Protein Eng. 15*, 373−82.
22. De Genst, E., Areskoug, D., Decanniere, K., Muyldermans, S., and Andersson, K. (2002) Kinetic and affinity predictions of a protein−protein interaction using multivariate experimental design, *J. Biol. Chem. 277*, 29897−907.
23. Desmyter, A., Transue, T. R., Ghahroudi, M. A., Thi, M. H., Poortmans, F., Hamers, R., Muyldermans, S., and Wyns, L. (1996) Crystal structure of a camel single-domain VH antibody fragment in complex with lysozyme, *Nat. Struct. Biol. 3*, 803−11.
24. Karlsson, R., Fagerstam, L., Nilshans, H., and Persson, B. (1993) Analysis of active antibody concentration. Separation of affinity and concentration parameters, *J. Immunol. Methods 166*, 75−84.
25. Canutescu, A. A., Shelenkov, A. A., and Dunbrack, R. L., Jr. (2003) A graph-theory algorithm for rapid protein side-chain prediction, *Protein Sci. 12*, 2001−14.
26. Brooks, B. R., Bruccoleri, R. E., Olafson, B. D., States, D. J., Swaminathan, S., and Karplus, M. (1983) CHARMM: A program for macromolecular energy, minimization, and dynamics calculations, *J. Comput. Chem. 4*, 187−217.
27. Schaefer, M., Vlijmen, H. W. v., and Karplus, M. (1998) Electrostatic contributions to molecular free energies in solution, *Adv. Protein Chem. 51*, 1−57.
28. Schaefer, M., Sommers, M., and Karplus, M. (1997) pH-dependence of protein stability: Absolute electrostatic free energy differences between conformations, *J. Phys. Chem. B 101*, 1663−83.
29. Davis, M. E., Madura, J. D., Luty, B. A., and McCammon, J. A. (1991) Electrostatics and diffusion of molecules in solution: Simulations with the University of Houston Brownian Dynamics program, *Comput. Phys. Commun. 62*, 187−97.
30. van Vlijmen, H. W. T., Schaefer, M., and Karplus, M. (1998) Improving the accuracy of protein pK_a calculations: Conformational averaging versus the average structure, *Proteins: Struct., Funct., Genet. 33*, 145−58.
31. Beroza, P., Fredkin, D. R., Okamura, M. Y., and Feher, G. (1991) Protonation of interacting residues in a protein by a Monte Carlo method: Application to lysozyme and the photosynthetic reaction center of *Rhodobacter sphaeroides*, *Proc. Natl. Acad. Sci. U.S.A. 88*, 5804−8.
32. Tanford, C., and Roxby, R. (1972) Interpretation of protein titration curves. Application to lysozyme, *Biochemistry 11*, 2192−8.
33. Lowe, C. R. (1999) Chemoselective biosensors, *Curr. Opin. Chem. Biol. 3*, 106−11.
34. Zhou, H. X. (2001) Disparate ionic-strength dependencies of on and off rates in protein−protein association, *Biopolymers 59*, 427−33.
35. Schreiber, G. (2002) Kinetic studies of protein−protein interactions, *Curr. Opin. Struct. Biol. 12*, 41−7.
36. Walker, D., Moore, G. R., James, R., and Kleanthous, C. (2003) Thermodynamic consequences of bipartite immunity protein binding to the ribosomal ribonuclease colicin E3, *Biochemistry 42*, 4161−71.
37. Xavier, K. A., and Willson, R. C. (1998) Association and dissociation kinetics of anti-hen egg lysozyme monoclonal antibodies HyHEL-5 and HyHEL-10, *Biophys. J. 74*, 2036−45.
38. Marvin, J. S., and Lowman, H. B. (2003) Redesigning an antibody fragment for faster association with its antigen, *Biochemistry 42*, 7077−83.
39. Huang, H. C., and Briggs, J. M. (2002) The association between a negatively charged ligand and the electronegative binding pocket of its receptor, *Biopolymers 63*, 247−60.
40. Paynter, S., and Russell, D. A. (2002) Surface plasmon resonance measurement of pH-induced responses of immobilized biomolecules: Conformational change or electrostatic interaction effects? *Anal. Biochem. 309*, 85−95.
41. Livesay, D. R., and Subramaniam, S. (2004) Conserved sequence and structure association motifs in antibody-protein and antibody-hapten complexes, *Protein Eng., Des. Sel. 17*, 463−72.
42. Transue, T. R., De Genst, E., Ghahroudi, M. A., Wyns, L., and Muyldermans, S. (1998) Camel single-domain antibody inhibits enzyme by mimicking carbohydrate substrate, *Proteins 32*, 515−22.
43. Lafont, V., et al., unpublished data.
44. Freyhult, E. K., Andersson, K., and Gustafsson, M. G. (2003) Structural modeling extends QSAR analysis of antibody-lysozyme interactions to 3D-QSAR, *Biophys. J. 84*, 2264−72.
45. Tanokura, M. (1983) ^{1}H NMR study on the tautomerism of the imidazole ring of histidine residues. I. Microscopic p*K* values and molar ratios of tautomers in histidine-containing peptides, *Biochim. Biophys. Acta 742*, 576−85.
46. Umetrics AB (2003) *Modde 7: User Guide and Tutorial*, Umetrics AB, Umeå, Sweden.

BI050986V